Heavy-ion-beam-induced laser scheme in hydrogenlike He^+

M. Salvermoser, A. Ulrich, and J. Wieser
Technische Universität München, Fakultät für Physik E12, James Franck Strasse 1, D-85747 Garching, Germany
(Received 23 February 1998; revised manuscript received 15 June 1998)

A recombination laser scheme on the $\lambda = 164$ nm $n = 3-2$ transition in H-like He^{+*} ions is studied. Doubly ionized helium is produced in a 300-mbar He gastarget using a pulsed 110-MeV $^{32}S^{8+}$ heavy-ion beam. The cross section for this ionization process is 9.2×10^{-17} cm^2. Since the flux of existing heavy-ion accelerators is limited, plasmas generated directly by heavy-ion beams reach only an electron density n_e on the order of 10^{12} cm^{-3}. In order to study three body recombination of He^{2+} ions with free electrons, electron densities n_e of at least 10^{14} cm^{-3} and electron temperatures T_e well below 0.1 eV are necessary. In this study the required electron density is produced by means of a special gas discharge. Time evolution of the plasma parameters n_e and T_e in the plasma target prior to the arrival of the heavy-ion beam pulse is described by a numerical model. Light intensity on the 164-nm $n = 3-2$ transition following heavy-ion beam excitation is measured using time resolved optical spectroscopy. Light intensity on this spectral line and its dependence from electron density and temperature in the plasma is interpreted using a system of coupled rate equations modeling the He^{+*} system. [S1063-651X(98)08211-7]

PACS number(s): 52.40.Mj, 52.70.Kz

I. INTRODUCTION

There are two different approaches for obtaining population inversion in short wavelength lasers. On the one hand, there is the group of ion lasers [1,2], which require an ionizing nonequilibrium plasma as a laser medium. In this case the electron energy distribution function has a high energy component. These fast electrons are capable of populating the upper laser level by inelastic collisions. On the other hand, a recombinative nonequilibrium situation can be used to establish population inversion [3–5]. In this case the plasma has a high electron density n_e and a low electron temperature T_e, thus favoring recombination of highly charged ions with plasma electrons. The three body recombination process

$$X^{Z+} + 2e^- \rightarrow X^{(Z-1)+*} + e^- \tag{1}$$

between an ion (X) with charge state Z and two free electrons is the dominant recombination process. The rate of this reaction, R_{3K1} depends on the ion's charge Z and the plasma parameters n_e and T_e [6,7]:

$$R_{3K} = k_{3K} n_e^2 = 5.4\times10^{-27} \frac{Z^3}{T_e^{9/2}} n_e^2 \frac{\mathrm{eV}^{9/2}\,\mathrm{cm}^6}{\mathrm{s}}. \tag{2}$$

Since $R_{3K} \sim n_e^2 T_e^{-9/2}$ a high electron density n_e and a low electron temperature T_e are required for a high three body recombination rate. The recombining electron is caught in highly excited Rydberg-states, and subsequently deexcited via fast collisional deexcitation.

Recombination laser systems with wavelengths as short as the extreme vacuum ultraviolet (XUV, $\lambda \leqslant 100$ nm) were predicted as early as 1965 [3], and demonstrated successfully many times [8,9]. In these cases, high power laser pulses were used to generate dense, hot plasmas ablated from the surface of solid targets (e.g., carbon), which dissipate energy very quickly by adiabatic expansion and radiation cooling. For a short time during this very dynamic plasma evolution process, plasma parameters are favorable for establishing population inversion by recombination of highly charged ions with cooled free electrons.

An alternative approach for producing supercooled recombining plasmas using a heavy-ion beam stopped in a rare-gas target ($p \approx 1000$ mbar) is proposed here. The main aspect for using heavy-ion beams are the high cross sections for producing highly charged target ions [10,11]. This collisional ionization process is nonthermal, and the recoil target ions have a very low kinetic energy [12]. As a result, heavy-ion beams have the potential for producing plasmas with high densities of multiply charged ions embedded in a cold environment of neutral target atoms or dense low temperature plasmas. In heavy-ion beam driven plasmas, a large percentage of the energy deposition in the target is stored in the form of ionization energy of ground state target ions. There are several ways to channel this energy reservoir into a certain laser transition.

On the one hand, the target ions can react with the surrounding cold target atoms. This is the case in all heavy-ion beam pumped lasers up to now, since the beam current of heavy-ion accelerators is rather limited. As a result, electron densities produced directly by heavy-ion collisions are too low for obtaining significant three body recombination rates with free electrons. The degree of ionization χ by this process is presently only on the order of $\chi \approx 10^{-6}$. As a consequence, the target ions produced predominantly form charged excimers with the surrounding cold target gas atoms. These charged rare-gas excimer molecules recombine via dissociative recombination with free electrons, leaving one atom in an excited state. Recombination of molecular ions in heavy-ion beam excited gas targets was investigated by Ribitzki *et al.* [13], and is instrumental for establishing population inversion in heavy-ion beam pumped lasers [14,15].

On the other hand, it is possible to channel the potential energy directly into ionic transitions, if the ions are sur-

rounded by a high electron density. These can be quasifree, weakly bound electrons from donor atoms (for example, Cs atoms) which are mixed with the target gas at a sufficiently high density [16]. The upper level in such laser schemes is efficiently populated by selective charge transfer reactions between a heavy-ion beam produced target ion and a donor atom.

As the beam intensity increases, electron density in the target increases as well, leading to a high three body recombination rate of free electrons with heavy-ion beam produced target ions. This way, ionization energy stored in the ground state ions is channeled efficiently into highly excited ionic levels, making recombination laser schemes possible.

Motivated by the development of high intensity heavy-ion accelerators such as the high intensity development program at the Gesellschaft für Schwerionenforschung in Darmstadt [17], it will be possible to produce high specific power densities in the target. This will lead to degrees of ionization of $\chi = 10^{-4}$ and more. Based on predictions using the model described here, these intense heavy-ion beams will create plasma parameters in the target, suitable for quasi-*dc* (10–80 ns pulses) recombination lasers around 100 nm.

For studying this situation in advance, a special plasma target has been developed providing a high electron density ($n_e \approx 10^{14}$ cm^{-3}) by using a gas discharge in a 300-mbar helium-gas target. The target can be operated in two modes, with discharge on and off. In both cases light on the $\lambda = 164$ nm ($n = 3 \rightarrow 2$) transition in H-like He^+ induced by the heavy-ion beam pulse is observed using time resolved optical spectroscopy. Light on this transition without a plasma target is used as a reference for heavy-ion beam induced light output with plasma target on. At delay times between 100 and 500 ns after igniting the discharge, a 100-MeV $^{32}S^{8+}$ heavy-ion beam pulse of 2-ns duration was sent into the plasma target, efficiently producing He^{2+} ions. A model has been developed which describes the temporal development of plasma parameters in the plasma target up to the arrival of the heavy-ion beam pulse. Production of He^{2+} ions in an environment created by the plasma target leads to an increase of ion beam induced population density in the He^{+*} ($n = 3$) level due to three body recombination of He^{2+} ions with free plasma electrons. This level is also populated directly in collisions of the projectiles with the He atoms in the target gas. In the experiment we compare the light output on the $\lambda = 164$ nm He^{+*} ($n = 3 \rightarrow 2$) transition induced directly by heavy-ion beam excitation (discharge switched off) with the light intensity with the plasma target activated leading to additional population via the recombination process. An increase in light output of 40% in case of the plasma target activated was observed. The increase of population density in the He^{+*} ($n = 3$) level due to three body recombination of He^{2+} ions can be described using a model for temporal development of plasma parameters in the discharge plasma and a system of rate equations for H-like He^{+*}.

The transition studied is one of the typical recombination laser transitions in H-like ions in the XUV spectral region [8]. The scheme described here can therefore be scaled to recombination laser schemes using more highly charged ions.

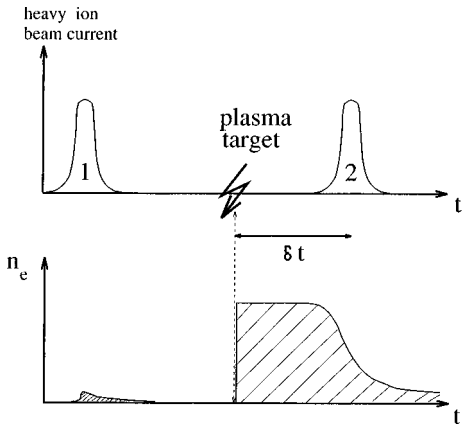

FIG. 1. Timing scheme used for the experiment: A first heavy-ion beam pulse preionizes the volume between two blade electrodes, and is used to provide a trigger signal for the plasma target a time interval δt before a second beam pulse arrives. This second beam pulse produces He^{2+} ions. Three body recombination of these ions with free electrons in the target plasma is studied.

II. EXPERIMENT

A. Ion beam

Experiments were performed at the Munich Tandem van de Graff accelerator. A pulsed beam of 110-MeV $^{32}S^{9+}$ ions was used for the excitation of a helium-gas target. Each pulse consisted of 10^6 particles and was focused to a beam spot of 0.8-mm diameter. The pulse width of each pulse was 2 ns. Pulses were formed using a pulsing system installed at the low energy side of the accelerator consisting of an electrostatic chopper and a double drift tube buncher. The instantaneous ion beam flux at the focus spot inside the target gas was 5×10^{16} cm^{-2} s^{-1}. The ion beam was sent into the gas target (helium, $p_{He} = 300$ mbar and $n_{He} = 10^{19}$ cm^{-3}) through a 1 mg/cm^2 titanium entrance foil of 4-mm aperture. Using a cross section measured by Berg [18], initial He^+ and He^{2+} densities of 10^{12} and 9×10^{10} cm^{-3} are produced in the target. The pulsing system was used with a pulsing sequence with 819.2-μs-delay time between ion beam pulses. Since the plasma target could only be operated with a repetition rate of 10 Hz, a heavy-ion beam pulse was selected every 100 ms to trigger the gas discharge. The time history of the experiment is schematically shown in Fig. 1. The first pulse preionized the gas. Then the plasma target was ignited for producing free electrons. The following ion beam pulse was used for the actual experiment. A capacitive pick-off producing a fast timing signal at the arrival of a beam pulse was installed in the beam line for triggering the discharge and data taking using adjustable delays.

B. Target cell and plasma target

A schematic drawing of the target cell is shown in Fig. 2. It was made from standard stainless steel high vacuum components with a 100-mm tube diameter. Two 40-mm-long knive-edge shaped tungsten electrodes were mounted in the center of the cell. They were separated by 1 mm and carefully aligned with respect to the ion beam axis. The final adjustment of the beam was performed during the experiment using steerer magnets in the beam line while observing the beam position with an alignment telescope through a

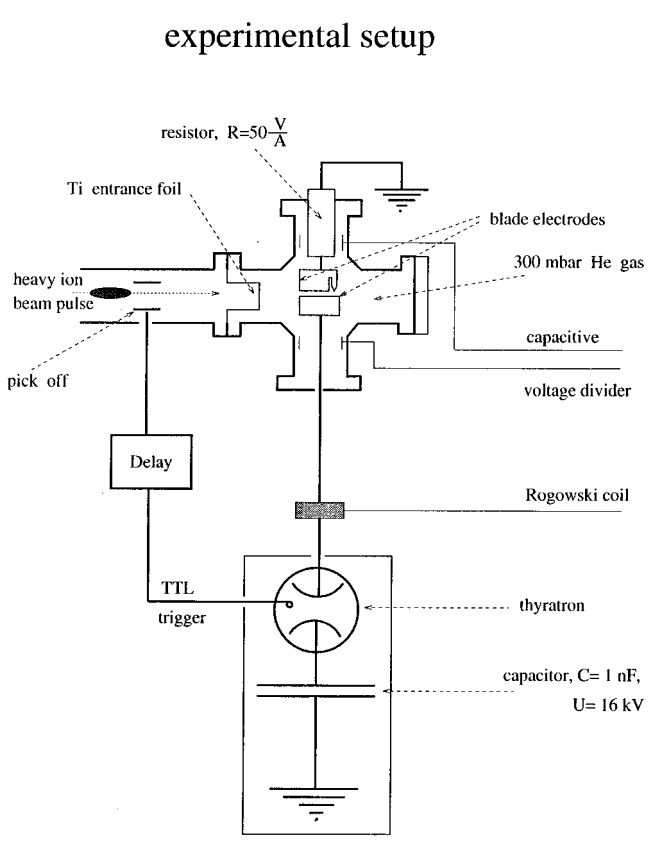

FIG. 2. Schematic drawing of the experimental setup: The target cell, beam line, discharge region, and electrical ignition systems are shown.

viewing port at the end of the cell. The electrodes were held by insulating mounts made from teflon. Wherever possible the electrical feed through was designed for a rf resistance of 50 Ω. A brass tube was placed around the blade electrodes and leads inside the cell for that purpose.

A modified power supply from a nitrogen laser was used as a driver for the discharge. Triggering was performed by a thyratron switch delivering a 16-kV pulse to the coaxial high voltage cable leading to the cell. The shape of the current pulse was measured using a Rogowski coil. Two capacitive probes were installed inside the cell for measuring the voltage drop across the discharge gap versus time.

The plasma target was designed as a special streamer discharge. The goal was to produce a homogeneously excited volume with an electron density n_e on the order of 10^{15} cm^{-3} and a low electron temperature T_e on the order of 0.1 eV.

The concept was to preionize the target volume with a first ion beam pulse. Then, with a delay of 819 μs, approximately 200 ns before the next heavy-ion beam pulse arrived, the high voltage pulse for the discharge was applied. Streamers in which the density of free electrons increases due to electron collisions develop in the electrical field between the electrodes. It is important to stop the streamer process rapidly for a cooling phase for the electrons to follow. This was achieved by an arc discharge which developed at one end of the blade electrodes. A separate sharp tip attached to the grounded electrode with a slightly shorter distance to the hot electrode than the knife edge part of the grounded electrode was used for that purpose. The arc discharge which essentially short circuited the electrodes typically 5 ns after ignition was optically well shielded from the diagnostic part of the setup.

An estimate of the average electron density n_e in the region adjacent to the anode, right after termination of the streamers by the arc as described above, can be obtained as follows. As long as the electrical field between the electrodes is on, electrons are accelerated by the external electrical field, causing collisional ionization of neutral helium atoms. The average distance an electron travels until it ionizes a helium atom is given by the inverse of the Townsend ionization coefficient α. In the streamer head, the external electrical field separates electrons and He^+ ions by a distance on the order of α^{-1}. This causes an internal polarization field E_{Pol} on the order of

$$E_{\mathrm{Pol}} \approx \frac{e n_e \alpha^{-1}}{\epsilon_0}$$

which is in opposite direction to the external electrical field E_{extern}. [Here $e = 1.6 \times 10^{-19}$ A s, $\epsilon_0 = 8.85 \times 10^{-12}$ A s/Vm and $\alpha = (16\ \mu\mathrm{m})^{-1}$ is the first Townsend ionization coefficient in 300-mbar He gas [19].] If E_{Pol} compensates E_{extern}, electron multiplication stops. As a result, the average electron density in the region adjacent to the anode can roughly be estimated as follows:

$$\epsilon_0 E_{\mathrm{extern}} \approx e n_e \alpha^{-1}. \tag{3}$$

A peak voltage of 5 kV across the electrodes was measured using the two capacitive voltage probes. The average electric field within a distance of 200 μm of the knife edge anode is on the order of 230 kV/cm. This results in an estimated average electron density of 10^{14} cm^{-3} after termination of the streamer mechanism.

Estimate of the plasma parameters at the time of beam interaction

We emphasize that it is not our intention to model the discharge itself. Our goal is to estimate the development of n_e and T_e after the voltage between electrodes is switched off, in order to obtain the plasma parameters at the time of interaction with the heavy-ion beam. Modeling of the plasma parameters $n_e(t)$ and $T_e(t)$ starts at termination of the streamer development by the arc discharge outside the observed region. As discussed above, the streamer discharge produces an electron density on the order of 10^{14} cm^{-3} embedded in a sea of dense (10^{19} cm^{-3}), cold helium atoms. Due to inelastic collisions with helium atoms, the kinetic energy of the streamer electrons drops almost immediately (within less than a ns) below $E(\mathrm{He}\ 2\ ^3S_1) = 19.77$ eV, which is the lowest excitation energy of helium atoms. Afterwards the electrons couple closely to the cold, dense helium-gas environment by elastic collisions [see Eq. (5)]. Note that the coupling between the fast electrons themselves due to elastic coulomb scattering is weak ($\tau_{e-e}^{-1} \sim n_e T_e^{-3/2}$ [7]).

Since no explicit electron energy distribution function has been calculated for the discharge and early times after its termination, T_e should be regarded as the most likely kinetic electron energy right after termination of the streamer pro-

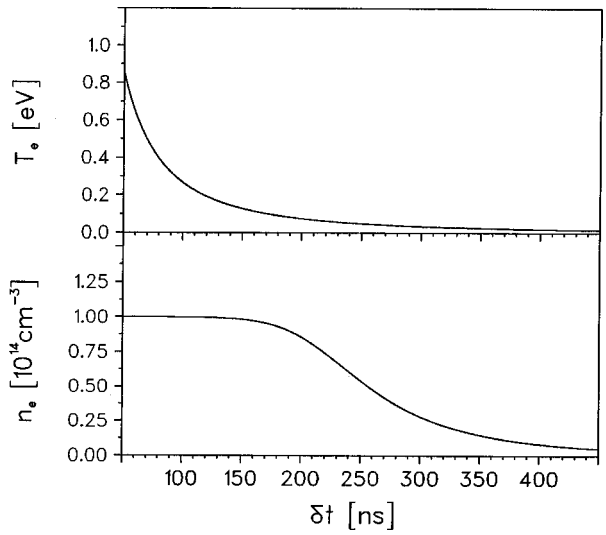

FIG. 3. Time evolution of electron temperature and density after termination of the electron producing streamer mechanism.

cess, and not as a temperature. After about 50 ns the electrons are considerably slower, and Coulomb scattering is finally strong enough to establish a Boltzmann distribution among the electrons, with T_e then representing the temperature of the electron ensemble. The time evolution of plasma parameters (n_e, T_e) is calculated by solving the rate equations (4). The result is shown in Fig. 3:

$$\frac{dT_e}{dt} = -(T_e - T_{\mathrm{He}})(\tau^E_{e-\mathrm{He}})^{-1} - (T_e - T_{\mathrm{He}^+})(\tau^E_{e-\mathrm{He}^+})^{-1}, \tag{4a}$$

$$\frac{dT_{\mathrm{He}}}{dt} = -[T_{\mathrm{He}} - T_{\mathrm{He}}(t=\infty)]\tau^{-1}_{\mathrm{Diff}}, \tag{4b}$$

$$\frac{dT_{\mathrm{He}^+}}{dt} = -(T_{\mathrm{He}^+} - T_{\mathrm{He}})(\tau^E_{\mathrm{He}^+-\mathrm{He}})^{-1} + (T_e - T_{\mathrm{He}^+}) \times (\tau^E_{e-\mathrm{He}^+})^{-1}, \tag{4c}$$

$$\frac{dn_e}{dt} = -k_{3K} n_{\mathrm{He}^+} n_e^2 - k_{\mathrm{Diss}} n_{\mathrm{He}_2^+} n_e - \tau^{-1}_{\mathrm{Diff}} n_e, \tag{4d}$$

$$\frac{dn_{\mathrm{He}^+}}{dt} = -k_{3K} n_e^2 n_{\mathrm{He}^+} - k_{\mathrm{Ex}} n_{\mathrm{He}}^2 n_{\mathrm{He}^+} - \tau^{-1}_{\mathrm{Diff}} n_{\mathrm{He}^+}, \tag{4e}$$

$$\frac{dn_{\mathrm{He}_2^+}}{dt} = -k_{\mathrm{Diss}} n_e n_{\mathrm{He}_2^+} + k_{\mathrm{Ex}} n_{\mathrm{He}^+} n_{\mathrm{He}}^2 - \tau^{-1}_{\mathrm{Diff}} n_{\mathrm{He}_2^+}. \tag{4f}$$

The elastic energy exchange collision frequency used in Eq. (4a) between electrons and He atoms is [20]

$$(\tau^E_{e\text{-He}})^{-1} = \frac{2m_e}{m_{\mathrm{He}}} \sigma_{e\text{-He}} n_{\mathrm{He}} v_e \sim n_{\mathrm{He}} \sqrt{T_e}, \tag{5}$$

with $\sigma_{e\text{-He}} = 5 \times 10^{-16}$ cm^2. The corresponding expression for He-He$^+$-collisions (4c) is

$$(\tau^E_{\mathrm{He}^+\text{-He}})^{-1} = \frac{3}{8} \sigma_{\mathrm{He}^+\text{-He}} n_{\mathrm{He}} v_{\mathrm{He}} = \left(2.93 \times 10^{-11} \frac{\mathrm{cm}^3}{\mathrm{s}}\right) n_{\mathrm{He}} \left(\frac{T_{\mathrm{He}^+}}{\mathrm{eV}}\right)^{1/2},$$

with $\sigma_{\mathrm{He}^+\text{-He}} = 10^{-16}$ cm^2.

The electrons and He$^+$ ions are thermally coupled by elastic Coulomb scattering processes [$(\tau^E_{e\text{-He}^+})^{-1}$; see Eqs. (4a) and (4c) and Ref. [7]]. The decrease of n_e and n_{He^+} in the volume studied due to ambipolar diffusion processes ($\tau_{\mathrm{Diff}} = 200$ ns [21]) is also taken into account [see Eq. (4b)]. The He gas in the streamers is heated up to 50 meV by the streamer process, and cools exponentially with a decay time $\tau_{\mathrm{Diff}} = 200$ ns down to 27 meV (approximately equal to room temperature). The decay of electron density is mainly caused by three body recombination of electrons with He$^+$ ions [Eqs. (4d), (4e), and (4f)]. Formation of ionic He_2^+ molecules (k_{Ex} [22]) and their dissociative recombination with free electrons (k_{diss} [23]) is also included [Eqs. (4f), (4d) and (4e)]. With the setup operated at a repetition rate of 10 Hz, it was possible to obtain a very homogeneous sheet discharge between the blade electrodes which was analyzed using the diagnostic setup described below.

C. Diagnostics

The ion beam and discharge excited gas target was diagnosed using time resolved optical spectroscopy on the 164-nm vacuum ultraviolet (VUV) line of He$^+$. Light emitted perpendicular to the ion beam axis was focused onto the entrance slit of a ($f = 30$ cm) VUV monochromator (McPherson model 218). A 1:1 imaging optics consisting of a flat and a curved (radius of curvature 513.4 mm) Al-MgF_2 coated mirror was designed using a ray tracing program. The entrance slit of the monochromator was oriented parallel to the slit between the discharge electrodes. A resolution of the imaging optics of 100 μm was obtained.

A MgF_2 window was installed at the diagnostics port of the target cell. The entire light path outside the cell was evacuated to better than 10^{-4} mbar. Focusing and alignment of the optics was performed by 3-micrometer mirror mounts of the flat mirror. Light emitted from the arc discharge between the tip of the upper electrode to the lower one was carefully shielded by a cage made from carbon fiber plates inside the target cell. A phototube with a MgF_2 entrance window (Thorn EMI 9426B) mounted at the exit port of the VUV monochromator was used as a detector. Measurements of light intensity were performed in the current mode of the phototube terminated by a 50-Ω resistor for obtaining ns time resolution. The output signal was recorded using a 300-MHz dual trace storage oscilloscope (Tektronix 2440) with 1024 data points storage depth. A typical setting during the measurements was 100 ns per division and 5 mV per division, respectively. Data were averaged over 256 discharge pulses using the oscilloscope, and transferred to a computer for further analysis as described below. The absolute sensitivity of the detection system used was known from earlier work.

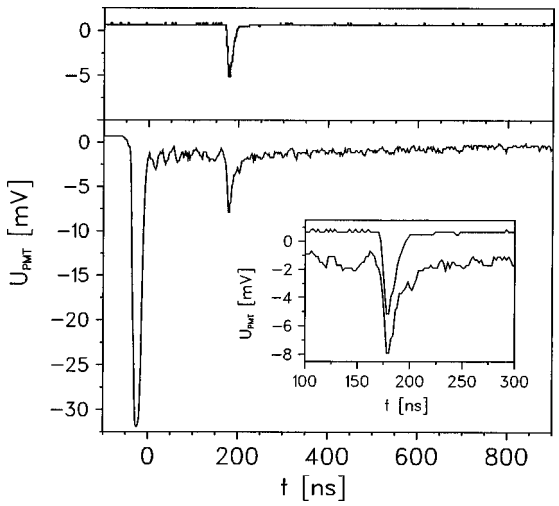

FIG. 4. Light emission on the 164-nm He^{+*} ($n=3\rightarrow 2$) transition is shown vs time *without* (above) and *with* an active (below) plasma target. In the lower part of the figure, the pulses are induced by the discharge (left) and the ion beam pulse (right), respectively. The inset shows an expanded view of the phototube signal induced by the ion beam pulse.

III. EXPERIMENTAL RESULTS

A. Data analysis

The experimental setup described above could be operated routinely during experimental runs with repetition rates of the discharge up to 10 Hz. The crucial part of the design was to develop a discharge which enhanced the initial electron density $n_e \approx 10^{12}$ cm^{-3} provided by preionization by two orders of magnitude without arcing. With all requirements met, a typical phototube signal as recorded on the 164-nm He^+ line has a time dependence like the one shown in Fig. 4.

In the upper part of Fig. 4, a heavy-ion beam pulse excites a 300-mbar He-gas target without a discharge. The $He^+ n=3$ level is populated by collisional excitation of target atoms by the heavy ion projectiles. The full width at half maximum of the phototube signal is 8 ns.

In the lower part of Fig. 4, the heavy-ion beam pulse interacts with the plasma target. The first intense signal is due to collisional ionization and collisional excitation into the $n=3$ level of He^+ during the discharge phase. Note that the streamer mechanism is no thermal ionization process, and results in a nonthermal plasma. The arc discharge following the initial voltage pulse shows only a small, slowly decaying signal with some ringing on it, due to some electrical mismatch either in the discharge or the phototube circuit. A very homogeneous light blue sheet discharge was observed between the knife edge electrodes and a bright arc discharge at the tip of the electrodes. Without proper alignment or at much higher gas pressure, etc., arcing occurred between the knife edge part of the electrodes. Under such conditions the light emitted from the arcs dominated the signal. Note, that not a single case of arcing is allowed to occur during the 256 discharge pulses needed to record an intensity versus time plot as the one shown in Fig. 4. This means the probability for arcing had to be on the order of 10^{-4} or lower for reasonable data taking.

The signal in Fig. 4 not yet discussed is the second peak ($t \approx 200$ ns), which shows the 164-nm light pulse induced by heavy-ion beam excitation. A similar light pulse is also observed without the discharge, as shown in the upper part of Fig. 4. Absolute intensity measurements of the light emission without discharge allow the optical emission cross section for the 164-nm transition to be measured. The photon emission rate per atom normalized to the flux of incident heavy-ion projectiles independent of the specific processes leading to light emission (direct excitation into the upper level, cascades from higher lying levels etc.). A value of $(9\pm 5)\times 10^{-20}$ cm^2 was obtained for the $n=3-2$ transition for the 100-MeV ^{32}S ions used in the experiment, with the sensitivity of the detection system being the main source of experimental error.

An important aspect in studying the recombination in the plasma target is a precise measurement of the time integrated heavy-ion beam induced light intensity at least on a relative scale. Data without ignition of the discharge were used as a reference. Such reference data were recorded before and after each measurement, with the discharge applied to the target gas. The ion beam intensity was measured using a Faraday cup behind the plasma target, and continuously monitored on a chart recorder. Sets of data where beam fluctuations of more than 20% occurred were not included in the data analysis. Integration of the normalizing intensity could be performed easily since no background signal was observed. With the discharge activated, the beam induced light signal is overlayed by the background signal of the discharge. The following procedure was used to accurately measure the time integrated ion beam induced light intensity. The decay of the discharge light with the beam switched off was described using the following relation with seven free parameters a_0-a_6:

$$Y_D(t)=a_0\exp(-a_1 t)+a_2\exp(-a_3 t)\sin(a_4 t+a_5)+a_6. \tag{6}$$

The first term describes the exponential decay of the fraction of light from the arc discharge which reaches the detector despite shielding. The second term takes electronic ringing into account. An offset is represented by parameter a_6. The onset and decay of the ion beam induced light was modeled by

$$Y_{B+}(t)=a_7\{\tanh[a_8(t-a_9)]+1\}\exp[-a_{10}(t-a_9)]. \tag{7}$$

The hyperbolic tangent term is used to describe the sharp onset of the light signal induced by the ion beam pulse, and the exponential function its slower decay. The sum of these two functions was fitted to the experimental data. The time of the onset of the ion beam pulse, which was varied experimentally as described below, could also be varied in the model by adjusting the parameter a_9. The result of such a data analysis is shown in Fig. 5. Experimental data, the corresponding fit function, and their difference (residuum) is plotted versus time. The residuum shows only white noise, indicating that the function describes the data properly. The onset and decay of the ion beam induced light without plasma target was modeled by the function

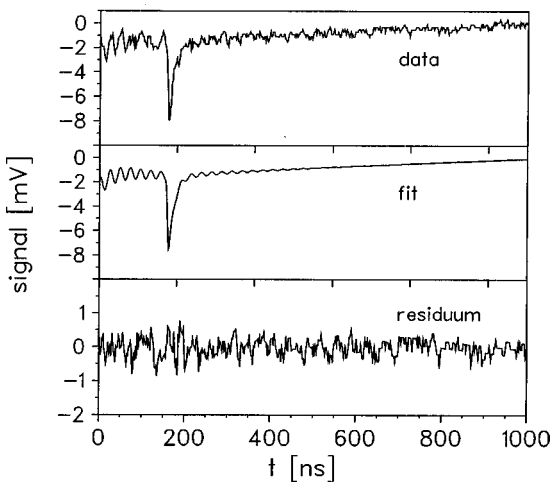

FIG. 5. Phototube signal of ion beam pulse induced light emission on the 164-nm ($n=3\rightarrow2$) transition in He^{+*} (data), with fit and resulting residuum (termination of discharge at $t=0$).

$$Y_{B-}(t)=a_7\{\tanh[a_8(t-a_9)]+1\}\exp[-a_{10}(t-a_9)]+a_6, \tag{8}$$

completely analogous to Eq. (7).

Numerical integration could then be performed on the ion beam part of the model, resulting in an accurate measure of the time integrated light signal induced by the ion beam without plasma target I_- (164 nm) and with plasma target I_+(164 nm) for various discharge conditions:

$$I_-(164\ \text{nm})=\int_0^\infty Y_{B-}(t)dt, \tag{9}$$

$$I_+(164\ \text{nm})=\int_0^\infty Y_{B+}(t)dt. \tag{10}$$

The relative increase in the time integrated heavy-ion beam induced light signal on the $\lambda=164$ nm $He^{+*}(n=3\rightarrow2)$ transition is then used as a signature for three body recombination S_{3K}:

$$S_{3K}=\frac{I_+(164\ \text{nm})}{I_-(164\ \text{nm})}. \tag{11}$$

Experimental errors were determined as follows. The error due to photon statistics is about 7%. The error introduced by the data acquisition system is dominated by the jitter in electron multiplication in the phototube. This can be treated purely statistically as well, and is on the order of 8%. Both contributions have been taken into account for both the signal and normalization data, as discussed below.

Experimental results for the signature $S_{3K}(\delta t)$ for three body recombination with the heavy-ion beam, interacting with the plasma target at a time δt after termination of the streamer mechanism, are shown in Fig. 6. Different symbols indicate that data were measured at different experimental runs with completely new settings of the Tandem accelerator, showing that the results were nicely reproducible.

Data can be qualitatively interpreted as follows. When the heavy-ion beam pulse is sent into the plasma target too early

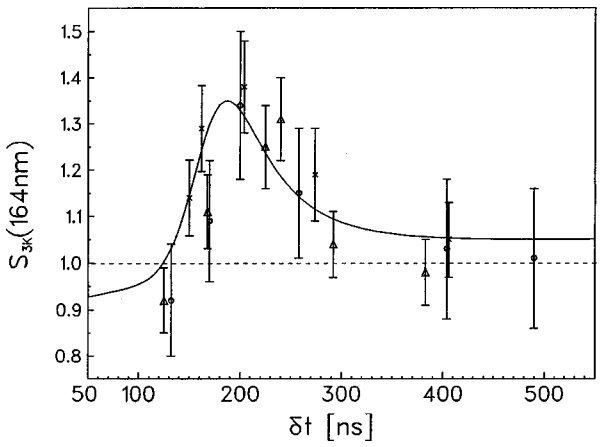

FIG. 6. Relative increase in the light output for the He^{+*} ($n=3\rightarrow2$) transition due to three body recombination of heavy-ion produced He^{2+} ions with free electrons supplied by the plasma target. Calculated signature S_{3K}, as defined in the text, is also shown.

($\delta t\leqslant150$ ns), then the electrons are too hot and three body recombination is not significant ($R_{3K}\sim n_e^2T_e^{-9/2}$). Around $\delta t=200$ ns the electron density n_e is still high, and the electron temperature T_e is low enough for three body recombination of heavy-ion beam induced He^{2+} ions to occur. In this process the $He^{+*}(n=3)$ level is populated directly by the heavy-ion beam and additionally by three body recombination, leading to an increase in the light output on the $He^{+*}(n=3\rightarrow2)$ transition. At $\delta t=200$ ns, an increase in integrated light intensity of about 40% is observed. This results in a three body recombination rate $R_{3K}=3\times10^7$ s^{-1}. If $\delta t>200$ ns, then T_e is low in the plasma target, but n_e also decreases rapidly (see Fig. 3). Since $R_{3K}\sim n_e^2$, the three body recombination rate decreases, and the population of the $He^{+*}(n=3)$ level by three body recombination ceases too. Note that the data at $\delta t\approx130$ ns with $S_{3K}<1$ are real. They can be explained by the fact that at such short times after the discharge, there is a high electron density in the target plasma, which leads to a high rate of nonradiating collisional deexcitation of the $He^{+*}(n=3)$ level. At the same time, a high electron temperature hampers the population of this level by three body recombination of He^{2+} ions. Also, the temperature of the target gas is high right after termination of the streamer mechanism, which causes an adiabatic expansion of the target gas. This leads to a reduced target gas density, again adding to a decrease of heavy-ion beam induced light output on the $He^{+*}(n=3\rightarrow2)$ transition at early times.

B. Modeling of the data

Experimental data shown in Fig. 6 can be explained using coupled rate equations describing the He^{+*} system. The rate equation (12) was solved numerically, providing the time dependent population densities without $[n_{3-}(t)]$ and with $[n_{3+}(t)]$ an active plasma target. The heavy-ion beam pulse was treated as a δ function in time where $j_B\approx10^8$ cm^{-2} instantaneously producing population densities $n_{He^{+*}(m)}(t=0)$ for main quantum numbers $3\leqslant m\leqslant6$ and $n_{He^{2+}}$ with

cross sections σ_m and $\sigma_{He^{2+}}=9.2\times10^{-17}$ cm^2 [18]. Cross sections $\sigma_3=4.3\times10^{-19}$ cm^2 and $\sigma_4=1.5\times10^{-19}$ cm^2 have been measured using an absolutely calibrated monochromator-detector system. The other cross sections have been calculated according to

$$\frac{\sigma_n}{\sigma_m}=\frac{f_{1,n}^{\mathrm{abs}}E_{1,m}}{f_{1,m}^{\mathrm{abs}}E_{1,n}},$$

with $f_{1,m}^{\mathrm{abs}}$ taken from Ref. [24].

If the beam pulse is sent into the 300-mbar He gas without a plasma target, $n_e=10^{12}$ cm^{-3} and $T_e=27$ meV are used in Eq. (12):

$$n_e=n_e(\delta t),$$

$$T_e=T_e(\delta t),$$

$$n_{He^{2+}}(t=0)=\sigma_{He^{2+}}n_{He}j_B,$$

$$n_m(t=0)=\sigma_m n_{He}j_B,\quad 3\leqslant m\leqslant 6,$$

$$\frac{dn_{He^{2+}}(t)}{dt}=-R_{3K}(T_e,n_e)n_{He^{2+}},$$

$$\frac{dn_6(t)}{dt}=R_{3K}(T_e,n_e)n_{He^{2+}}-\left(\sum_{i=1}^{5}(A_{6,i}+R_{6,i}^{\mathrm{Deex}})+k_P(6)n_{He}\right)n_6(t),$$

$$\frac{dn_5(t)}{dt}=(A_{6,5}+R_{6,5}^{\mathrm{Deex}})n_6(t)-\left(\sum_{i=1}^{4}(A_{5,i}+R_{5,i}^{\mathrm{Deex}})+k_P(5)n_{He}\right)n_5(t),$$

$$\frac{dn_4(t)}{dt}=\sum_{i=5}^{6}(A_{i,4}+R_{i,4}^{\mathrm{Deex}})n_i(t)-\left(\sum_{i=1}^{3}(A_{4,i}+R_{4,i}^{\mathrm{Deex}})+k_P(4)n_{He}\right)n_4(t),$$

$$\frac{dn_3(t)}{dt}=\sum_{i=4}^{6}(A_{i,3}+R_{i,3}^{\mathrm{Deex}})n_i(t)-\left(\sum_{i=1}^{2}(A_{3,i}+R_{3,i}^{\mathrm{Deex}})+k_P(3)n_{He}\right)n_3(t). \quad (12)$$

Due to the fast process of deexcitation induced by electron collisions ($R_{n,m}^{\mathrm{Deex}}$, as taken from Ref. [6]), three body recombination [$R_{3K}(T_e,n_e)$; see Eq. (2)] is treated as if recombination would occur directly into the $He^{+*}(n=6)$ level. The spontaneous emission rates between the levels ($A_{n,m}$) are taken from Ref. [24]. Penning ionization is taken into account by $k_P(n)$ given in Ref. [25]. Charge transfer rates between He^{2+} ions and He atoms, as well as the rate of He_2^{2+} molecule formation, have been estimated, and can be neglected in comparison with the rates of spontaneous emission, Penning ionization, and electron collisional deexcitation.

The time integrated intensity emitted on the $\lambda=164$ nm He^{+*} transition without plasma target [I_- (164 nm)] is proportional to the number of photons emitted per volume element $n_{\mathrm{Ph}-}$ (164 nm), and calculated according to

$$I_-\ (164\ \mathrm{nm})\sim n_{\mathrm{Ph}-}\ (164\ \mathrm{nm})=\int_0^{8\ \mathrm{ns}}A_{3,2}n_{3-}(t)dt. \quad (13)$$

When the beam pulse is sent into the active plasma target at a time δt after termination of the streamer mechanism, plasma parameters $n_e(\delta t)$ and $T_e(\delta t)$, as calculated using Eq. (4) and shown in Fig. 3, are used in Eq. (12):

$$I_+\ (164\ \mathrm{nm})(\delta t)\sim n_{\mathrm{Ph}+}\ (164\ \mathrm{nm})=\int_0^{8\ \mathrm{ns}}A_{3,2}n_{3+}(t)dt. \quad (14)$$

Applying the same analysis as performed for the experimental data [see Eq. (11)] to the intensities $A_{3,2}$ calculated by the theoretical model described above, leads to

$$\tilde{S}_{3K}(\delta t)=\frac{I_+\ (164\ \mathrm{nm})(\delta t)}{I_-\ (164\ \mathrm{nm})}=\frac{\int_0^{8\ \mathrm{ns}}A_{3,2}n_{3+}(t)dt}{\int_0^{8\ \mathrm{ns}}A_{3,2}n_{3-}(t)dt}. \quad (15)$$

Photons emitted more than 8 ns after the heavy-ion beam excitation were not included in the analysis since these photons could not be separated from background produced by the plasma target itself (see Figs. 4 and 5). In order to compare $\tilde{S}_{3K}(\delta t)$ with the measured relative increase in light output of the $He^{+*}(n=3\rightarrow2)$ transition (see Fig. 6), one has to take into account that the plasma target has a much smaller diameter ($\varnothing_{\mathrm{PT}}=200$ μm) than the heavy-ion beam ($\varnothing_{\mathrm{HIB}}=800$ μm), which leads to a smaller value of $S_{3K}(\delta t)$, since the influence of three body recombination I_{3K} (164 nm) on I_+ (164 nm) [see Eq. (14)] scales according to

$$I_{3K}\ (164\ \mathrm{nm})=\frac{\varnothing_{\mathrm{PT}}}{\varnothing_{\mathrm{HIB}}}[I_+\ (164\ \mathrm{nm})-I_-\ (164\ \mathrm{nm})]. \quad (16)$$

As a result, $\tilde{S}_{3K}(\delta t)$ has to be corrected as follows:

$$S_{3K}(\delta t)=\left(1-\frac{\varnothing_{\mathrm{PT}}}{\varnothing_{\mathrm{HIB}}}\right)+\frac{\varnothing_{\mathrm{PT}}}{\varnothing_{\mathrm{HIB}}}\tilde{S}_{3K}(\delta t)=0.75+0.25\tilde{S}_{3K}(\delta t). \quad (17)$$

Results of model data [$S_{3K}(\delta t)$; see Eq. (17)] and experimental data are compared in Fig. 6. Calculations are based on the modeling of plasma parameters $n_e(t)$ and $T_e(t)$ in the plasma target [see Eq. (4)] and rate equation (12) for the $He^{+*}(n)$ levels. As can be seen from Fig. 6, the measured

values of the signature S_{3K} for three body recombination, as well as its development with time, are accurately described by the model calculations.

ACKNOWLEDGMENTS

This work was funded by the German Federal Ministery for Research and Technology (BMBF) under Contract No. 06 TM 310 I, Gesellschaft für Schwerionenforschung (GSI), Darmstadt, the Tandem Accelerator Laboratory Munich, and NATO (Grant No. CRG 921215). The authors acknowledge help from B. Russ and H. Hagn in designing and building the plasma target, as well as valuable discussions with D. E. Murnick (Rutgers University). We also acknowledge the helpful support of the staff of the Tandem Accelerator Laboratory, Munich.

[1] W. E. Bell, Appl. Phys. Lett. **4**, 34 (1964).
[2] W. B. Bridges, Appl. Phys. Lett. **4**, 128 (1964).
[3] L. I. Gudzenko and L. A. Shelepin, Dokl. Akad. Nauk **160**, 1296 (1965) [Sov. Phys. Dokl. **10**, 147 (1965)].
[4] O. R. Wood II and W. T. Silfvast, Appl. Phys. Lett. **41**, 121 (1982).
[5] S. I. Yakovlenko, Laser Phys. **1**, 565 (1991).
[6] B. Kärcher, Ph.D. dissertation, Max-Planck-Institut für Quantenoptik, 1991.
[7] A. Anders, *A Formulary for Plasma Physics* (Akademie-Verlag, Berlin, 1990).
[8] S. Suckewer, C. H. Skinner, H. Milchberg, C. Keane, and D. Voorhees, Phys. Rev. Lett. **55**, 1753 (1985).
[9] G. Jamelot, A. Klisnick, A. Carillon, H. Guennou, A. Sureau, and P. Jaeglé, J. Phys. B **18**, 4647 (1985).
[10] C. L. Cocke, Phys. Rev. A **20**, 749 (1979).
[11] S. Kelbch, J. Ullrich, R. Mann, P. Richard, and H. Schmidt-Böcking, J. Phys. B **18**, 323 (1985).
[12] R. E. Olson, J. Ullrich, and H. Schmidt-Böcking, J. Phys. B **20**, L809 (1987).
[13] G. Ribitzki, A. Ulrich, B. Busch, and W. Krötz, Phys. Rev. E **50**, 3973 (1994).
[14] A. Ulrich, H. Bohn, P. Kienle, and G. J. Perlow, Appl. Phys. Lett. **42**, 782 (1983).
[15] A. Ulrich, J. Wieser, A. Brunnhuber, and W. Krötz, Appl. Phys. Lett. **64**, 1902 (1994).
[16] A. Ulrich, R. Gernhäuser, W. Krötz, J. Wieser, and D. E. Murnick, Phys. Rev. A **50**, 1931 (1994).
[17] I. Hofman, Nucl. Instrum. Methods Phys. Res. A **278**, 271 (1989).
[18] H. E. Berg, Ph.D. dissertation, Universität Frankfurt (1993); H. Berg, J. Ullrich, E. Bernstein, M. Unverzagt, L. Spielberger, J. Euler, D. Schardt, O. Jagutzki, H. Schmidt-Böcking, R. Mann, P. H. Mokler, S. Hagmann, and P. D. Fainstein, J. Phys. B **25**, 3655 (1992).
[19] L. M. Chanin and D. G. Rork, Phys. Rev. **133**, 1005 (1964).
[20] D. E. Golden and H. W. Bandel, Phys. Rev. **138**, 14 (1965).
[21] L. I. Reichl, *A Modern Course in Statistical Physics* (Academic, San Diego, 1990).
[22] A. V. Phelps and S. C. Brown, Phys. Rev. **86**, 102 (1952).
[23] J. N. Bradlsey and M. A. Biondi, Adv. At. Mol. Phys. **6**, 2 (1970).
[24] W. L. Wiese and G. A. Martin, *Wavelengths and Transition Probabilities for Atoms and Atomic Ions, Part II: Transition Probabilities*, Natl. Stand. Ref. Data System, Natl. Bur. Stand. (U.S.) Circ No. 68 (U.S. GPO, Washington, D.C., 1980).
[25] B. F. Smirnov and O. B. Firsov' Pis'ma Zh. Eksp. Teor. Fiz. **2**, 478 (1965) [JETP Lett. **2**, 297 (1965)].